Julie Dusseault,[1] Bing Li,[1] Nida Haider,[1] Marie-Anne Goyette,[2] Jean-François Côté,[2] and Louise Larose[1]

Nck2 Deficiency in Mice Results in Increased Adiposity Associated With Adipocyte Hypertrophy and Enhanced Adipogenesis

Diabetes 2016;65:2652–2666 | DOI: 10.2337/db15-1559

OBESITY STUDIES

Obesity results from an excessive expansion of white adipose tissue (WAT) from hypertrophy of preexisting adipocytes and enhancement of precursor differentiation into mature adipocytes. We report that *Nck2*-deficient mice display progressive increased adiposity associated with adipocyte hypertrophy. A negative relationship between the expression of Nck2 and WAT expansion was recapitulated in humans such that reduced Nck2 protein and mRNA levels in human visceral WAT significantly correlate with the degree of obesity. Accordingly, Nck2 deficiency promotes an adipogenic program that not only enhances adipocyte differentiation and lipid droplet formation but also results in dysfunctional elevated lipogenesis and lipolysis activities in mouse WAT as well as in stromal vascular fraction and 3T3-L1 preadipocytes. We provide strong evidence to support that through a mechanism involving primed PERK activation and signaling, Nck2 deficiency in adipocyte precursors is associated with enhanced adipogenesis in vitro and adiposity in vivo. Finally, in agreement with elevated circulating lipids, *Nck2*-deficient mice develop glucose intolerance, insulin resistance, and hepatic steatosis. Taken together, these findings reveal that Nck2 is a novel regulator of adiposity and suggest that Nck2 is important in limiting WAT expansion and dysfunction in mice and humans.

In humans, obesity is a strong determinant condition for the development of metabolic disorders such as type 2 diabetes. Obesity is characterized by an excessive expansion of white adipose tissue (WAT) that relies on hypertrophy of preexisting adipocytes and the generation of mature adipocytes through growth and differentiation of preadipocytes after adipogenesis (1). At the molecular level, adipogenesis is regulated by a timely transcriptional network involving CCAAT-enhancer–binding protein (C/EBP) transcription factors, with C/EBPδ and β in the early stages of differentiation, whereas C/EBPα in concert with peroxisome proliferator–activated receptor-γ (PPARγ) promotes adipocyte maturation. A genome-wide association study for adiposity in the Framingham cohort found, as expected, single nucleotide polymorphisms in well-characterized adipocyte markers, such as *PPARG* and *ADIPOQ* (2). Of note, among significant single nucleotide polymorphisms associated with adiposity, this study also identified rs10496393 in the gene area encoding of the Src homology (SH) domain containing adaptor protein Nck2.

In mammals, two genes encode for the closely related Nck1 and Nck2 proteins, which are essentially composed of SH domains with three N-terminal SH3 and one C-terminal SH2 domains (3). Nck proteins are well-known to assemble molecular complexes that mediate canonical signaling from activated membrane receptors regulating cytoskeletal reorganization (4,5). In addition, Nck1 and Nck2 are implicated in noncanonical signaling pathways through their ability to regulate the unfolded protein response (UPR) (6–8). The UPR is initiated at the level of the endoplasmic reticulum (ER) by three ER transmembrane sensors: the double-stranded RNA-like ER kinase (PERK), Ser/Thr kinase/endoribonuclease inositol–requiring enzyme-1α (IRE1α), and activating transcription factor 6 (ATF6) (9). We and others implicated Nck in regulating the UPR through its interaction with the β-subunit of the eukaryotic initiation factor 2 (eIF2β) (8,10,11), Ser/Thr phosphatase PP1 (8,12), PERK (13,14), and IRE1α (7). We demonstrated that Nck1

[1]Department of Medicine, McGill University, and McGill University Health Centre Research Institute, Montreal, Quebec, Canada
[2]Institut de Recherches Cliniques de Montréal (Université de Montréal), Montreal, Quebec, Canada
Corresponding author: Louise Larose, louise.larose@mcgill.ca.

Received 10 November 2015 and accepted 9 June 2016.

is essential for sustained hepatic activation of the IRE1α-JNK pathway associated with impaired glucose homeostasis secondary to obesity in mice (15). We also have showed that Nck1 modulates PERK-dependent regulation of insulin biosynthesis and survival in pancreatic β-cells (13,14). In the current study, we report that Nck2 is required to regulate PERK activity and signaling during adipogenesis and in mature adipocytes to prevent abnormal WAT expansion and dysfunction associated with metabolic disorders.

RESEARCH DESIGN AND METHODS

Animal Studies

Nck2$^{-/-}$ and *Nck2*$^{+/+}$ mouse littermates were generated as previously described (16). Male mice were used in all experiments according to approved protocol 5069 by the McGill University animal care committee.

Antibodies and Cells

The antibodies used were as follows: Hsp90 (4877S), Akt (9272), pAkt Thr^{308} (9275L), pAkt Ser^{473} (9271L), eIF2α (9722S), fatty acid synthase (FAS) (3180), aP2 (3544), adiponectin (2789), perilipin (9349), acetyl-CoA carboxylase (ACC) (3676), PERK (3192), and β-actin (4967S) from Cell Signaling Technology; PPARγ (sc-7196), ATF4 (sc-200), pPERK Thr^{980} (32577), and RasGAP (sc-63) from Santa Cruz Biotechnology; human Nck2 (TA307351) from Origene, PEPCK (1002S) from Cell Applications; peIF2αSer^{51} (44728G) from Invitrogen; Flag (3165) from Sigma; and Nck1 and panNck as previously described (10,15). The 3T3-L1 cell line from ATCC was cultured as recommended by the manufacturer.

Body Composition, Metabolic, and Serum Analyses

Fat mass was determined by DEXA (Lunar PIXImus II; GE Healthcare). Glucose (1–2 g/kg), insulin (0.75 units/kg), and sodium pyruvate (2 g/kg) were injected intraperitoneally, and blood glucose was quantified with an Accu-Chek glucometer (Roche). With use of a TSE PhenoMaster, metabolic parameters and locomotor activity were recorded according to the manufacturer. Commercial kits were used to determine serum insulin, tumor necrosis factor-α (TNF-α), interleukin (IL) 6, and adipokine levels (Meso Scale Discovery) as well as triglycerides (TGs) and nonesterified fatty acids (NEFAs) (Sigma). As recommended by the manufacturer, hepatic and skeletal muscle glycogen contents were evaluated using boiled tissue extracts and a glycogen assay kit from Sigma (MAK016).

Primary Cultures

Primary hepatocytes were prepared as previously described (17). Insulin dose response (10 and 100 nmol/L, 15 min) was performed 2 days after initial plating (18). To prepare the stromal vascular fraction (SVF), WAT depots were minced and digested with collagenase (1 mg/mL, C0130; Sigma). Digestion was stopped by adding ice-cold DMEM plus 10% FBS followed by successive centrifugation and filtration on prewet 70- and 40-μm cell strainers. SVFs were plated at 1×10^5 cells in six-well plates. At confluence, differentiation was induced with 1 μmol/L dexamethasone, 1 μmol/L rosiglitazone, 0.5 mmol/L 3-isobutyl-1-methylxanthine (IBMX), and 3 μg/mL insulin for 3 days and then maintained in the same medium but without IBMX for 4 days.

Immunoblotting

Tissues and cell extracts were prepared as previously reported (15). Total proteins (20–50 μg) were resolved by SDS-PAGE, transferred onto polyvinylidene fluoride, and immunoblotted with indicated antibodies. For Nck distribution, tissue extracts from *Nck1*$^{-/-}$ and *Nck2*$^{-/-}$ mice were normalized for protein content (50 μg) and processed similarly using panNck antibodies.

Adipocyte Differentiation, Small Interfering RNA, and Lipogenesis

Two days postconfluency, 3T3-L1 cells were differentiated by using a classical cocktail (1 μmol/L dexamethasone, 0.5 mmol/L IBMX, 1 μg/mL insulin) for 2 days and then incubated in DMEM plus 10% FBS containing only 1 μg/mL insulin for 2 days before being maintained in regular medium. For small interfering RNA (siRNA) experiments, 2 days before confluency, 3T3-L1 cells were reverse transfected with 1 nmol/L of Nck2 (Mouse)-3 unique 27mer siRNA duplexes (SR412820; Origene) using 7.5 μL Lipofectamine RNAiMAX Reagent (Invitrogen) in six-well plates. Lipid droplet formation was visualized using BODIPY 493/503 (Thermo Fisher Scientific) and confocal microscopy and quantified after oil red O (ORO) staining. For ORO staining, cells were fixed in 10% PBS-buffered formalin for 15 min, permeabilized using 60% isopropanol for 5 min, and stained with 0.18% ORO for 15 min. For quantification, ORO was eluted in 100% isopropanol for 10 min and read at 492 nm with a spectrophotometer (EnSpire 2300 Multilabel Plate Reader; PerkinElmer). For BODIPY 493/503, cells were incubated at 1 μg/mL for 10 min and wash twice before visualization with a confocal Zeiss microscope (LSM 510 META) or quantification using Infinite M200 PRO Tecan (excitation 500 nm, emission 550 nm). In vitro lipogenesis was assessed by using a classical oleate uptake protocol (19).

Cell Proliferation and Flow Cytometry Analysis

3T3-L1 cells Nck2 siRNA transfected or overexpressing Nck2 and their respective controls were plated at 5×10^3 cells/well in 24-well plates. MTT [3-(4,5-dimethylthiazol-2-yl)-2,5-diphenyltetrazolium bromide] activity was assessed to determine cell number on days 1–4 after plating as previously described (14). Freshly isolated WAT SVF from both mouse genotypes were washed twice and incubated for 30 min at 4°C with the following antibodies: PE/Cy7 CD29 (clone HMβ1-1; BioLegend 102221), allophycocyanin CD34 (clone HM34; BioLegend 128611), and Pacific Blue Sca-1 (clone D7; BioLegend 108119). After antibody incubation, cells were washed and analyzed on a BD FACSCanto II flow cytometer. For 3T3-L1 cells, after incubation with BODIPY (1 mg/mL) for 10 min at room temperature, cells were washed three times and analyzed using the same FACS analyzer.

Histology

Adipose tissues (7 μm) were embedded in paraffin and processed for hematoxylin and eosin (H&E) staining. Adipocyte density was quantified using ImageQuant (GE Healthcare Life Sciences). Hepatosteatosis was assessed by ORO staining. Livers were embedded in optimal cutting temperature matrix (CellPath) and kept at −80°C until analysis. Frozen liver sections (6 μm) were processed for ORO or H&E staining. Briefly, sections were dried for 10 min, rehydrated, and incubated for 30 min in 2% weight for volume ORO prepared in 50% acetone and 35% ethanol solution. Sections were counterstained with hematoxylin for 2 min.

RNA Extraction and Quantitative Real-Time PCR

Tissues were dissected and immediately snap frozen in liquid nitrogen for further analysis. RNA was extracted using TRIzol reagent (Invitrogen) according to manufacturer instructions. cDNA synthesis was performed by using a High-Capacity cDNA Reverse Transcription Kit (Applied Biosystems). Briefly, 1 μg of RNA was reverse transcribed in a master mix solution containing reverse transcriptase, random primers, deoxynucleotide (dNTPs), and RNase inhibitor. The reaction was carried out at 25°C for 10 min, 37°C for 120 min, and terminated at 85°C for 5 min. Quantitative real-time PCR was performed using Power SYBR Green PCR Master Mix (Applied Biosystems) and run on a ViiA 7 thermal cycler system (Applied Biosystems) using specific primers. Briefly, PCRs were performed for 40 cycles following 95°C for 15 s, 60°C for 30 s, and 72°C for 30 s. Expression levels were calculated using the ΔΔCt method, and data were normalized to housekeeping gene cyclophilin B, the expression of which did not vary among treatments. Specific primers for PCR amplification of targeted genes were used, and their sequences are available upon request.

RNA Sequencing

For both mouse genotypes, epididymal WAT (eWAT) total RNA (n = 2/genotype) was prepared as aforementioned and purified using RNeasy columns (QIAGEN). Expression libraries were generated using cBot clusters, and deep sequencing was performed using Illumina TruSeq RNA Sample Preparation Kit, Illumina TruSeq SR Cluster Kit v2, and Illumina TruSeq SBS Kit v2 (50 cycles) according to the manufacturer's procedures. Sequencing was performed at the Génome Québec Innovation Centre (McGill University) by using the Illumina HiSeq 2000 platform. Reads were aligned to the GRCm38 genome with TopHat v2.0.10, and the raw alignment counts were calculated with HTSeq v0.5.3. The differential expression measurements were performed with DESeq2 v1.4.5. The generation of the $Nck2^{-/-}$ signature was performed using DAVID v6.7 (Database for Annotation, Visualization and Integrated Discovery) (20,21) and GSEA v2.1.0 (Gene Set Enrichment Analysis) (22). For DAVID analyses, genes included in the studies had an adjusted $P < 0.10$ and an average differential expression of at least twofold. Principal component analyses of the gene expression data confirmed that the duplicates of the $Nck2^{+/+}$ and $Nck2^{-/-}$ samples respectively cluster together, whereas between genotypes, the samples were well separated from one another.

Insulin Release, Signaling, and Islet Content

Blood insulin levels before and after glucose (2 g/kg, 10 min) and insulin signaling (0.75 units/kg i.p., 15 min) in indicated tissues were assessed in overnight-fasted mice. Isolated pancreatic islets, as previously described (23), were subjected to an acid-ethanol extraction before determination of insulin content using radioimmunoassay (Linco Research) and expressed as normalized to DNA determined by SYBR Green.

Nck2 and PERK Overexpression and PERK Inhibitor

Upon transfection using Lipofectamine 2000 (Invitrogen) and G418 selection, stable pools of mock or Flag-Nck2 expressing 3T3-L1 cells were submitted to differentiation as aforementioned. Transient PERK wild-type overexpression was achieved after pcDNA3.1-PERK transfection using Lipofectamine 3000 (Invitrogen) 48 h before adipocyte differentiation. PERK inhibitor (GSK2606414) was added at 10 nmol/L during differentiation of 3T3-L1 cells.

Study Approval

Human subcutaneous WAT (scWAT) and omental WAT (oWAT) biopsy specimens from male subjects (BMI 35.5–69.8 kg/m^2) paired for age and date of bariatric surgery were obtained from the Biobank of Institut Universitaire de Cardiologie et de Pneumologie de Québec (IUCPQ), where written informed consent was obtained from the subjects according to institutionally approved management modalities. Study approval was obtained from the ethics committees of both IUCPQ and McGill institutions.

Statistics

Data from each group were compared by unpaired Student t test or two-way ANOVA using Prism software (GraphPad Software), and $P < 0.05$ was considered significant.

RESULTS

Nck2 Is Highly Expressed in Mouse WAT

Analysis of Nck protein expression in mouse tissues by Western blotting revealed that Nck1 is expressed in all tissues tested (Fig. 1*A*). In contrast, Nck2 is highly expressed in both lungs and eWAT and at very low levels in pancreas, brown adipose tissue (BAT), testis, and spleen, whereas it was not detected in other tissues tested (Fig. 1*A*). In addition, Nck2 is preferentially expressed in WAT compared with BAT, with the highest level in eWAT compared with scWAT (Fig. 1*B*).

Increased Adiposity and Adipokine Secretion in *Nck2*$^{-/-}$ Mice

Excluding the lungs, Nck2 is typically detected at high levels only in WAT, we used *Nck2* knockout mice to explore whether Nck2 plays a role in WAT. $Nck2^{-/-}$ mice displayed significantly larger WAT depots, whereas body weight, mouse size, and other tissues weight were

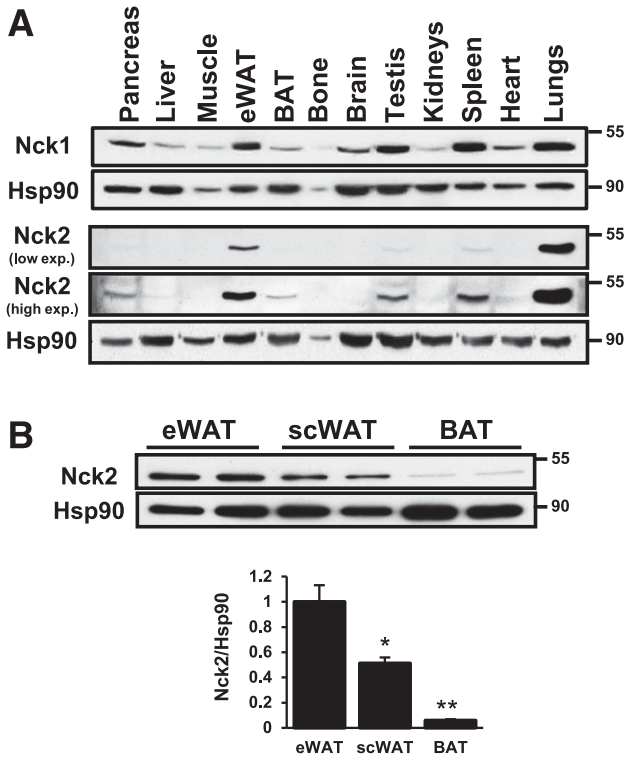

Figure 1—Nck2 is highly expressed in WAT. Western blot analysis of Nck1 and Nck2 expression in mouse tissues (*A*) and Nck2 expression in mouse adipose depots (*B*). Hsp90 was used as loading control. Data are mean ± SEM. $^*P < 0.05$, $^{**}P < 0.01$ by unpaired Student *t* test. exp., exposure.

comparable to $Nck2^{+/+}$mice (Fig. 2*A* and *B* and data not shown). Accordingly, DEXA confirmed a significant increase in total fat and fat mass in $Nck2^{-/-}$ mice, but lean mass was not changed (Fig. 2*C*). Total bone area was slightly, but not significantly, reduced in $Nck2^{-/-}$ mice compared with $Nck2^{+/+}$ mice (data not shown), potentially masking the impact of increased fat mass on total body weight. Increased adiposity in $Nck2^{-/-}$ mice was progressive (Fig. 2*D*), and analysis of eWAT at 24 weeks postweaning revealed adipocyte hypertrophy and reduced adipocyte density (Fig. 2*E*). Concomitantly, circulating levels of leptin and adiponectin were increased in $Nck2^{-/-}$ mice at 28 and 32 weeks postweaning, respectively (Fig. 2*F* and *G*). Of note, increased adiposity in $Nck2^{-/-}$ mice was not accompanied by inflammation as supported by identical TNF-α and IL-6 circulating levels compared with $Nck2^{+/+}$ mice. Furthermore, *Tnfa*, *Adrge1* (F4/80), and *Itgax* (Cd11c) mRNA levels were comparable between eWAT of both mouse genotypes (Fig. 2*H*). F4/80 staining showed no evidence of infiltrating macrophage-dependent formation of crown-like structure in expanded eWAT of $Nck2^{-/-}$ mice (data not shown). Collectively, the data demonstrate that WAT expansion in $Nck2^{-/-}$ mice is accompanied by adipocyte hypertrophy and enhanced release of adipokines but without any sign of inflammation.

Increased BMI Correlates With Reduced Nck2 Expression in Human Adipose Tissues

Increased adiposity in *Nck2*-deficient mice prompted us to assess whether WAT expansion in obese humans correlates with decreased Nck2 expression in WAT. Compared with both protein and mRNA levels in moderately obese subjects, Nck2 expression was reduced in oWAT of severely obese subjects (Fig. 3*A* and *B*). Nck2 protein levels were also lower in scWAT from severely obese subjects but did not reach statistical significance due to the limited number of samples analyzed. In contrast, Nck1 expression was comparable between groups and WAT depots (Fig. 3*A–C*), suggesting differential regulation of Nck proteins expression in WAT related to obesity. Altogether, these findings suggest a novel role for Nck2 in limiting WAT expansion in mice and humans.

Differential Gene Expression Profiles in $Nck2^{+/+}$ and $Nck2^{-/-}$ Mouse eWAT

To gain insight into the mechanisms that promote adiposity in $Nck2^{-/-}$ mice, we established differential gene expression profiles of eWAT between mouse genotypes by RNA sequencing (RNASeq). We focused on differentially expressed genes showing more than twofold significant change ($P < 0.05$): 1,420 and 2,472 genes were found upregulated and downregulated, respectively, in eWAT of $Nck2^{-/-}$ mice (National Center for Biotechnology Information Gene Expression Omnibus accession number GSE63510). Clustering function analysis of upregulated genes revealed changes in distinct functional networks related to adipocyte, lipid metabolism, obesity, and extracellular matrix (ECM) (Fig. 4*A*). mRNA levels of PPARγ (*Pparg*) and the proadipogenic transcription cofactor *Hairless* (*Hr*) were significantly increased in $Nck2^{-/-}$ mouse eWAT. Accordingly, PPARγ protein levels tend to increase in $Nck2^{-/-}$ mouse eWAT (Fig. 4*B*). RNASeq also revealed that the expression of PPARγ target genes (*Cebpa*, *Fabp4*, and *Fgf21*) and adipokine genes (*Lep*, *Adipoq*, and *Rbp4*) was induced in $Nck2^{-/-}$ mouse eWAT. In contrast, expression of early adipocyte differentiation regulators *C/EBPβ* and δ was not affected, suggesting that Nck2 regulates late events of adipocyte differentiation.

We next determined that the expression of genes involved in lipid metabolism, such as diacylglycerol acetyltransferase enzyme type 2 (*Dgat2*), PEPCK (*Pck1*), and several lipases (*Hsl*, *Atgl*, *Lpl*, and *Lipf*), and lipid droplet formation (*Cidec/FSP27*, *Cidea*, and *Plin4*) were significantly upregulated in $Nck2^{-/-}$ mouse eWAT. Furthermore, mesoderm-specific transcript (*Mest*) involved in adipocyte size regulation and adipose tissue expansion (24) was among the top upregulated genes in $Nck2^{-/-}$ eWAT. Genes previously identified as high-potential obesity candidates, including *Deptor*, *Thbs1*, *Tuba1a*, *Npr3*, and *Gys2* (25,26), were also significantly upregulated in $Nck2^{-/-}$ mouse eWAT. Consistent with the absence of inflammation in $Nck2^{-/-}$ mouse eWAT, *TNFa* and *IL6* mRNA levels were comparable in both mouse genotypes. RNASeq

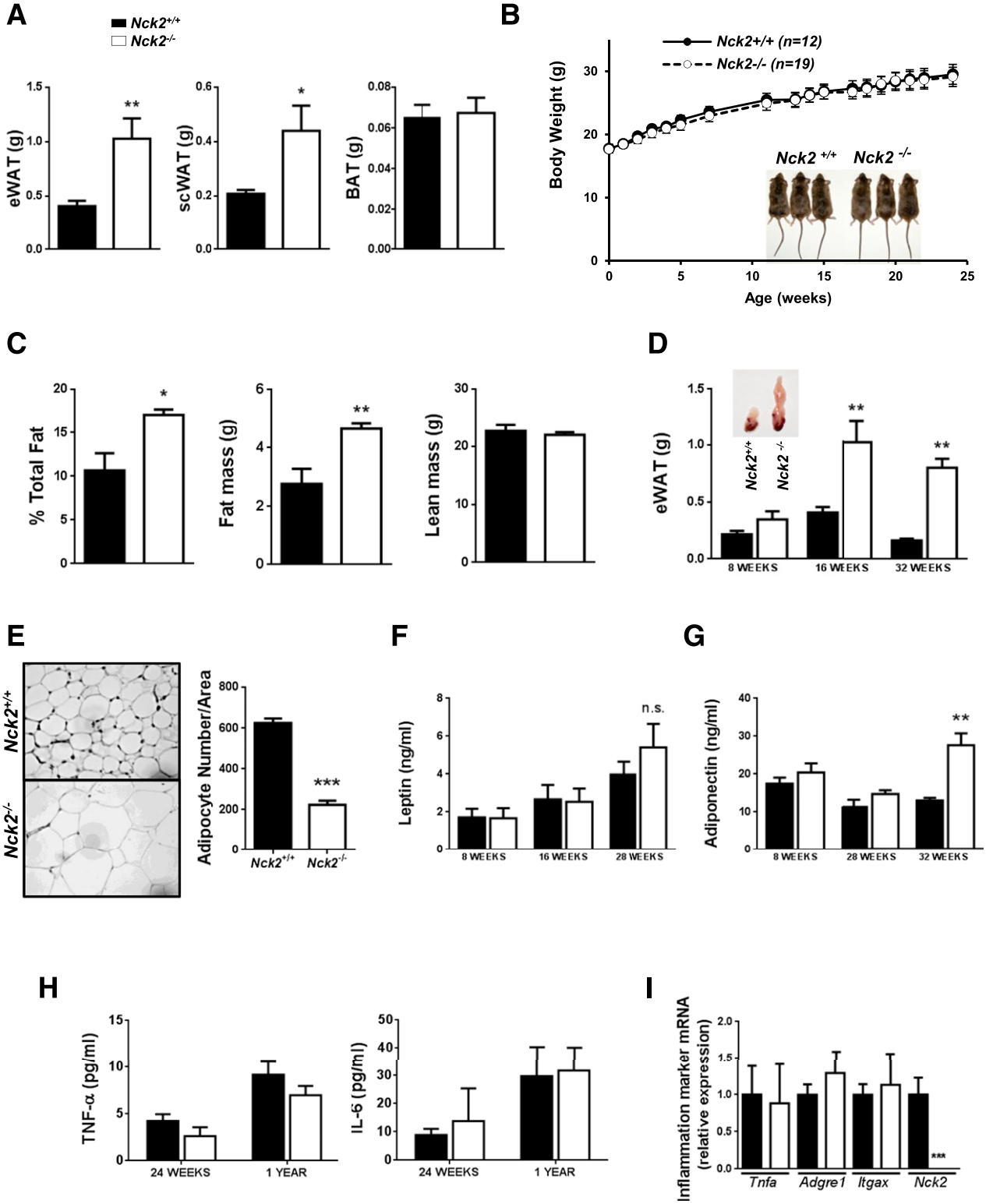

Figure 2—Increased adiposity and adipokine secretion in *Nck2*$^{-/-}$ mice. *Nck2*$^{-/-}$ mouse and *Nck2*$^{+/+}$ control littermate analysis included adipose tissue weight at 16 weeks postweaning (n = 5) (*A*), body weight (*B*) (inset shows image of mice), total fat and fat and lean mass at 32 weeks postweaning (n = 5) (*C*), eWAT weight (inset shows eWAT-testis image) (n = 5–10) (*D*), and eWAT H&E staining (original magnification ×40) and adipocyte density (n = 3–5) at 24 weeks postweaning (*E*). Blood levels of leptin (*F*), adiponectin (*G*), and TNF-α and IL-6 (n = 6–20) (*H*). *Tnfa*, *Adgre1*, *Itgax*, and *Nck2* mRNA levels in *Nck2*$^{+/+}$ and *Nck2*$^{-/-}$ mouse eWAT (n = 3) at 24 weeks postweaning (*I*). Data are mean ± SEM. *P < 0.05, **P < 0.01, ***P < 0.001 by unpaired Student t test. n.s., not significant.

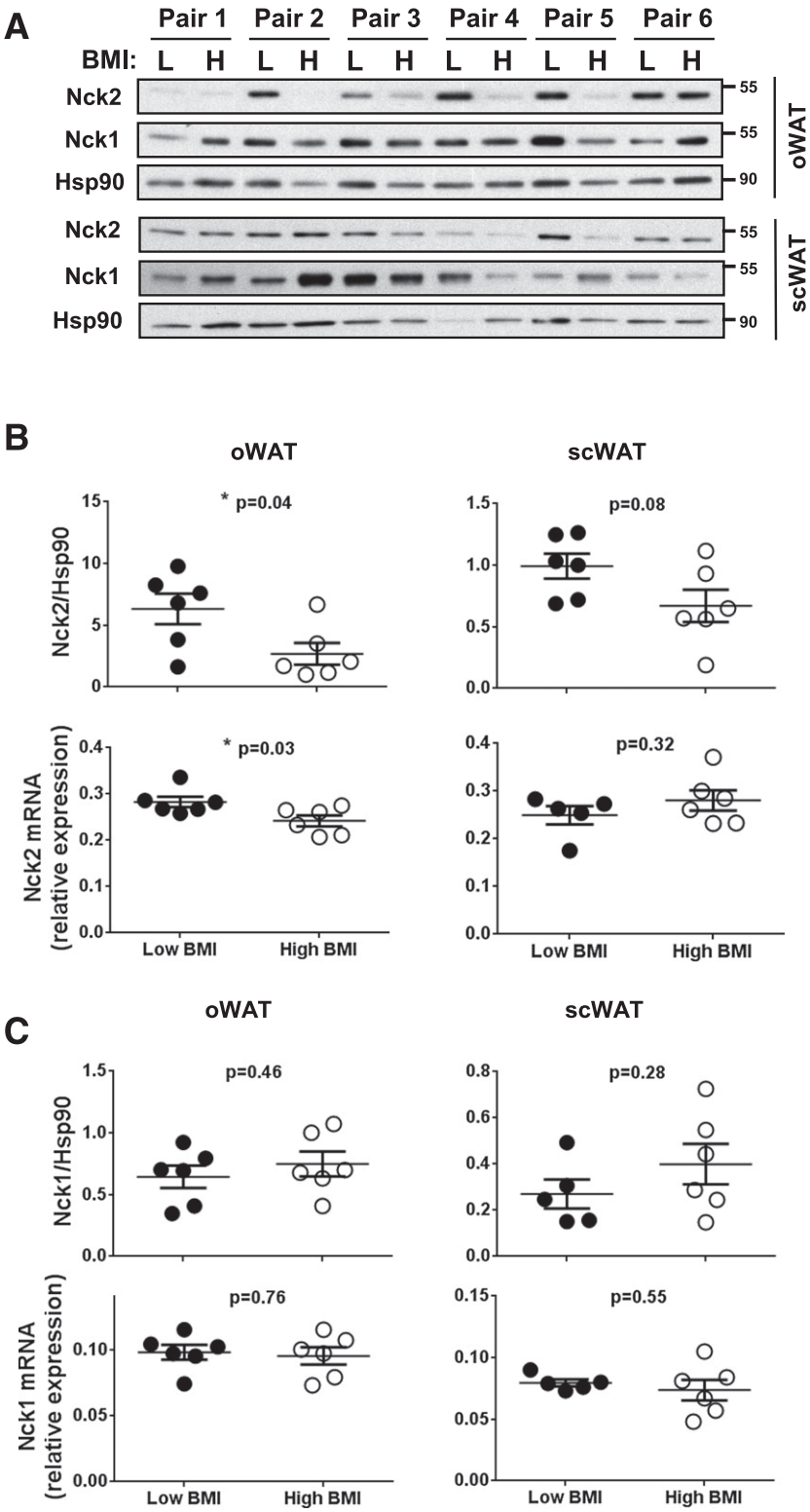

Figure 3— Increased BMI correlates with reduced Nck2 expression in human adipose tissues. Protein and mRNA expression levels of Nck2 (*A* and *B*) and Nck1 (*A* and *C*) in WAT of paired moderate (L, BMI <40 kg/m^2) to severely obese (H, BMI >60 kg/m^2) human subjects (n = 6/group). Data are mean ± SEM. *P < 0.05 by unpaired Student t test.

also revealed changes in the canonical Wnt pathway, which inhibits early steps of adipocyte differentiation (27,28). Expression of Wnt ligands was strongly downregulated, whereas *Sfrp5* encoding a Wnt signaling inhibitor (29) was greatly increased in eWAT of *Nck2*$^{-/-}$ mice. Increased levels of *Adipoq* gene expression in *Nck2*$^{-/-}$ eWAT were also

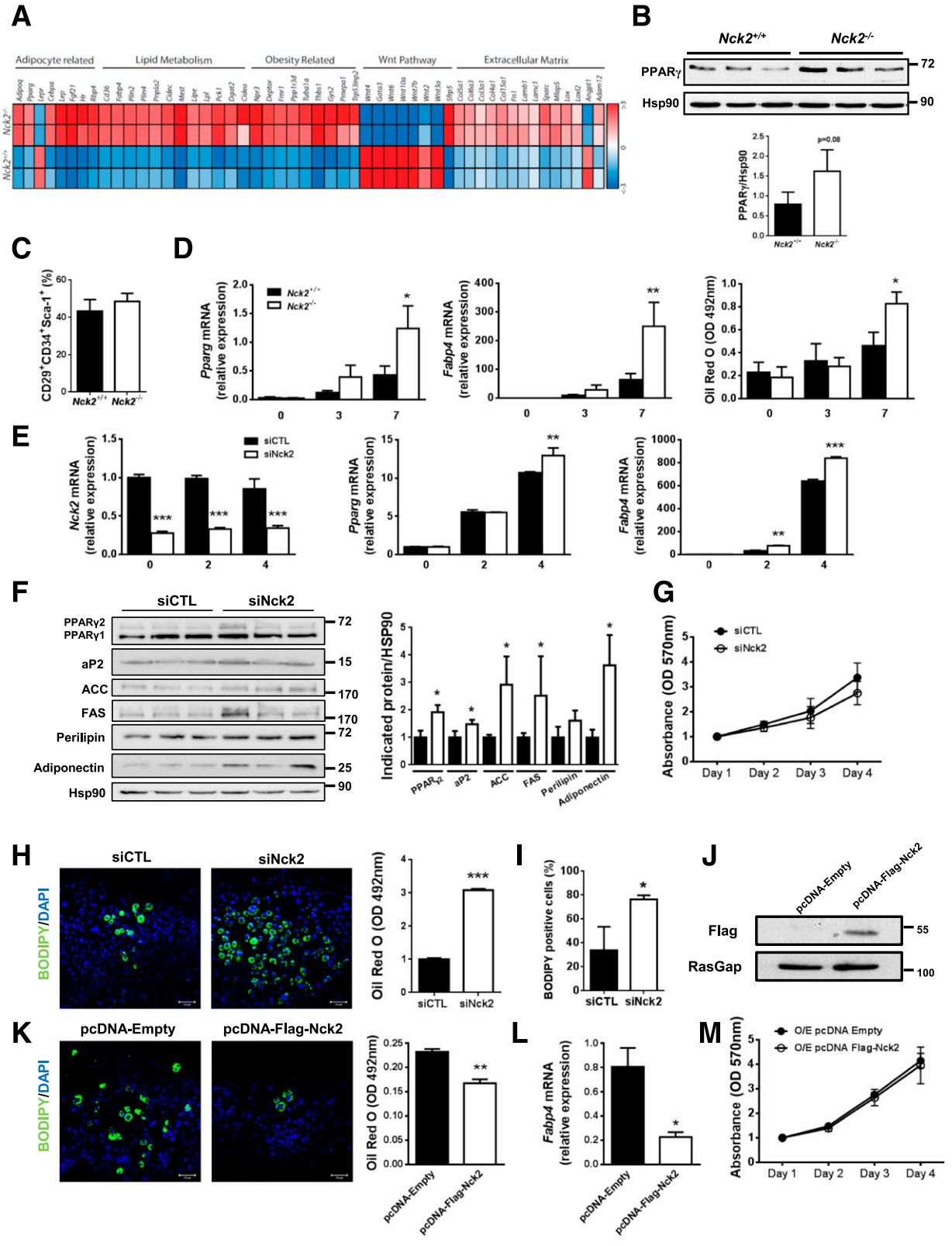

Figure 4—Nck2 regulates adipogenesis. Heat map of 51 genes differentially expressed between *Nck2*$^{-/-}$ and *Nck2*$^{+/+}$ mouse eWAT clustered to functional networks. Red indicates high expression and blue indicates low expression (*A*). PPARγ level in indicated mouse eWAT at 8 weeks postweaning (*B*). Percentage of adipocyte precursors (CD29^{+}CD34^{+}Sca-1^{+}) in scWAT SVF of both mouse genotypes (n = 6) (*C*). *Pparg* and *Fabp4* mRNA levels and ORO quantification at various time points during differentiation of *Nck2*$^{+/+}$ (n = 6) and *Nck2*$^{-/-}$ (n = 5) scWAT SVF (*D*). Indicated mRNA levels in control and Nck2 siRNA-treated 3T3-L1 cells during differentiation (n = 3) (*E*). Indicated protein levels in control and Nck2 siRNA-treated 3T3-L1 cells at day 4 of differentiation (*F*). Cell number assessed using an MTT assay in indicated siRNA-treated 3T3-L1 cells (n = 5) (*G*). Lipid accumulation (confocal image magnification ×10), ORO quantification, and BODIPY-positive cells

consistent with increased circulating adiponectin levels in *Nck2*$^{-/-}$ mice (Fig. 2*G*). In agreement with an important role for ECM remodeling in regulating preadipocyte commitment, numerous genes encoding ECM proteins (*Col5a1*, *Col15a1*, *Sparc*, and *Mfap5*) were significantly upregulated in *Nck2*$^{-/-}$ mice. Finally, we validated RNA-Seq data by quantitative real-time PCR for a selected set of genes and found concordance between both approaches (data not shown). Collectively, the findings strongly support a significant role for Nck2 in regulating the WAT adipogenic program.

Nck2 Deficiency Promotes Adipogenesis In Vitro

To further demonstrate that Nck2 regulates adipogenesis, we compared in vitro differentiation of primary adipocyte precursors in isolated SVF from both mice genotypes. *Nck2*-deficient WAT SVF, which contains equivalent percentages of adipocyte precursors (CD29^{+}CD34^{+}Sca-1^{+}) compared with *Nck2*$^{+/+}$ mice (Fig. 4*C*), showed enhanced differentiation as characterized by increased *Pparg* and *Fabp4* mRNA levels and ORO staining after 7 days of differentiation compared with *Nck2*$^{+/+}$ WAT SVF (Fig. 4*D*). We also confirmed that Nck2 regulates adipogenesis by silencing Nck2 in 3T3-L1 preadipocytes using siRNA, which decreased *Nck2* mRNA by ~70% for at least 4 days of differentiation. In fact, silencing Nck2 significantly promoted *Pparg* and *Fabp4* mRNA expression at day 4 of differentiation (Fig. 4*E*). In agreement, significantly higher levels of mature adipocyte markers: PPARγ_2, FABP4, adiponectin, and ACC were found in siRNA Nck2 3T3-L1 adipocytes (Fig. 4*F*). Evidence of increased fatty acid synthesis and lipid storage were suggested by higher levels of FAS, perilipin, and lipid droplet formation as assessed by ORO staining in Nck2-silenced 3T3-L1 cells (Fig. 4*F* and *H*). In addition, flow cytometry analysis demonstrated that the percentage of cells accumulating lipids was almost double upon silencing Nck2 in 3T3-L1 cells (Fig. 4*I*). Finally, silencing Nck2 in 3T3-L1 cells did not alter proliferation (Fig. 4*G*).

To assess whether Nck2 gain of function also affects adipogenesis, Nck2 was stably overexpressed in 3T3-L1 preadipocytes (Fig. 4*J*). In contrast to enhanced adipogenesis observed after silencing Nck2 in 3T3-L1, overexpression of Nck2 reduced 3T3-L1 differentiation as shown by a significant decrease in lipid droplet formation (Fig. 4*K*) and expression of *Fabp4* mRNA (Fig. 4*L*). As for silencing Nck2, stable overexpression of Nck2 in 3T3-L1 preadipocytes did not affect proliferation (Fig. 4*M*). Altogether, these results provide strong evidence in favor of a cell-autonomous role for Nck2 in regulating adipocyte differentiation.

Nck2 Deficiency Alters Adipocyte Function

To further support RNASeq data showing increased expression of genes involved in lipid metabolism in *Nck2*-deficient adipocytes, we compared expression of genes associated with adipocyte function in *Nck2*-deficient WAT SVF and Nck2-silenced 3T3-L1 adipocytes. mRNA levels of lipogenic enzymes, such as FAS (*Fasn*), ACC (*Acaca*), stearoyl-CoA desaturase 1 (*Scd1*), and fatty-acid elongation enzyme (*Elovl6*), were upregulated in *Nck2*$^{-/-}$-differentiated WAT SVF (Fig. 5*A*). Similarly, mRNA levels of these enzymes were increased in differentiated Nck2-silenced 3T3-L1 adipocytes (Fig. 5*B*). In addition, silencing Nck2 in 3T3-L1 preadipocytes significantly enhanced oleate-induced lipid droplet formation as monitored following BODIPY C16 uptake (Fig. 5*C*), indicating that Nck2 deficiency already affects lipogenic control in adipocyte precursor cells. Moreover, increased expression of lipid transporter genes *Cd36* and *Fabp4* in RNASeq of *Nck2*$^{-/-}$ mice eWAT, along with increased lipid droplet formation during differentiation of *Nck2*-deficient WAT SVF (Fig. 4*D*) and Nck2-silenced 3T3-L1 cells (Fig. 4*H*), strongly suggests a role for Nck2 in mature adipocyte lipid metabolism.

Like for lipogenic enzymes, genes encoding lipolytic enzymes, such as hormone-sensitive lipase (*Lipe*), adipose triglyceride lipase (*Atgl*), and monoacylglycerol lipase (*Mgl*), were strongly upregulated in both *Nck2*$^{-/-}$ WAT SVF and Nck2-silenced 3T3-L1 adipocytes (Fig. 5*D* and *E*). To determine whether increased lipolytic enzyme gene expression in *Nck2*-deficient adipocytes affect WAT homeostasis, we subjected mice to prolonged fasting periods and followed changes in body weight and weight of adipose tissue depots. Upon 24-h fasting, *Nck2*$^{-/-}$ mice showed greater loss in body weight and weight of eWAT and scWAT compared with *Nck2*$^{+/+}$ mice (Fig. 5*F*). However, these differences were less robust upon 48-h fasting, and no difference in BAT loss was noticed between mouse genotypes at any time. Thus, despite bigger WAT depots, *Nck2*$^{-/-}$ mice display accelerated loss of WAT upon fasting, suggesting increased in vivo lipolysis in agreement with increased expression levels of lipolytic enzymes. Moreover, fed plasma TGs (Fig. 5*G*) and NEFAs (Fig. 5*H*) were significantly elevated in *Nck2*$^{-/-}$ mice, revealing failure in lipid storage and/or increased lipolysis in *Nck2*$^{-/-}$ mice. Altogether, these data provide strong evidence that *Nck2* deficiency in mice, in addition to promoting adipogenesis, alters adipocyte function by increasing lipogenesis and lipolysis, both of which potentially contribute to elevated circulating lipid levels.

in control and Nck2 siRNA 3T3-L1 cells at day 4 of differentiation (n = 3) (*H* and *I*). Stable overexpression of Flag-tagged murine Nck2 in 3T3-L1 preadipocytes (*J*). Control and Flag-tagged Nck2 3T3-L1 at day 20 of differentiation (confocal image magnification ×10) and ORO quantification (*K*). *Fabp4* mRNA levels at day 15 of differentiation (n = 4) (*L*). Cell number assessed using an MTT assay in indicated 3T3-L1 cells (n = 3) (*M*). Data are mean ± SEM. *P < 0.05, **P < 0.01, ***P < 0.001 by unpaired Student t test. OD, optical density; O/E, overexpression; siCTL, control siRNA; siNck2, Nck2 siRNA.

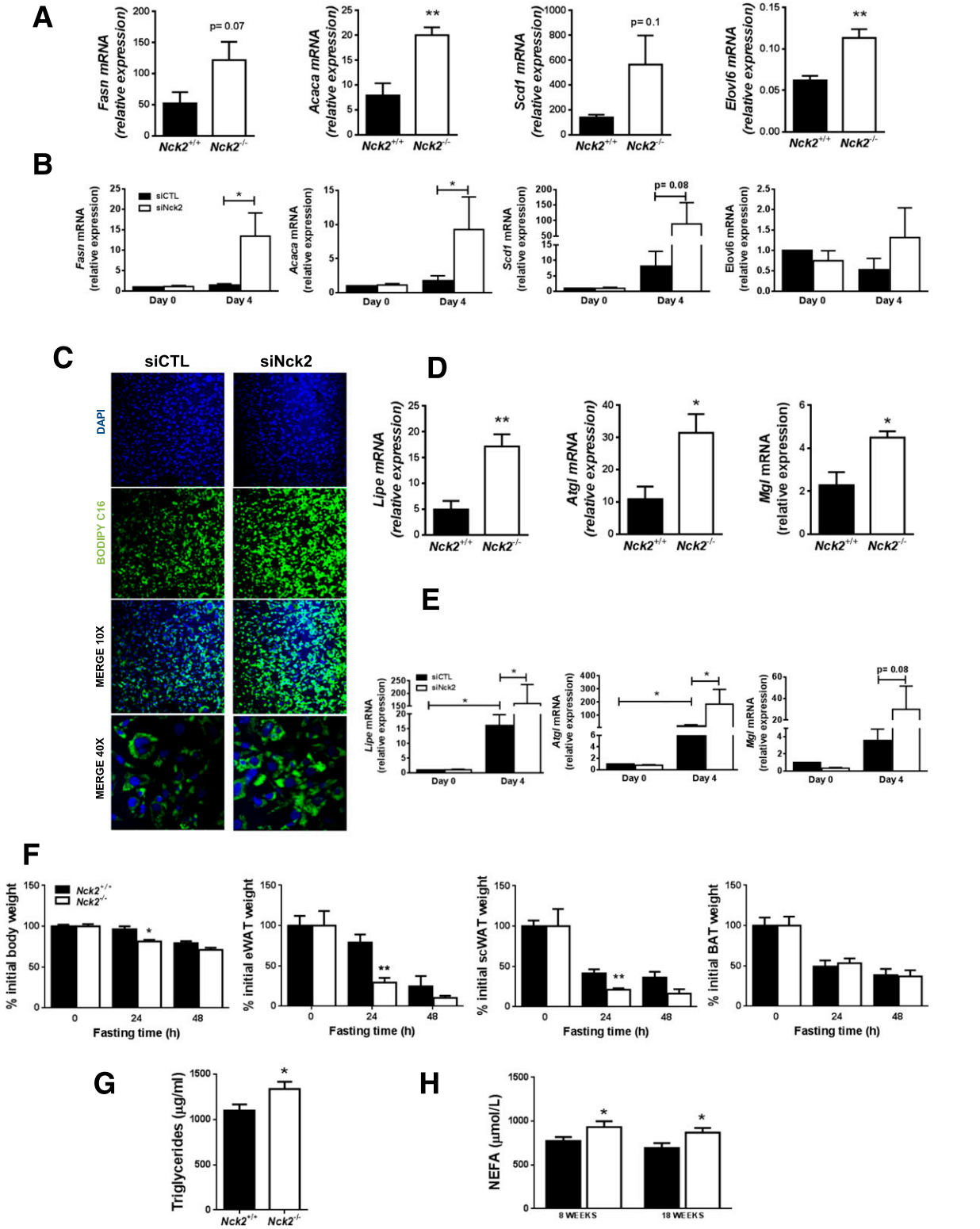

Figure 5—Nck2 deficiency alters adipocyte function. mRNA levels of indicated lipogenic genes in $Nck2^{+/+}$ (n = 6) and $Nck2^{-/-}$ (n = 5) WAT SVF after 7 days of differentiation (*A*) and control and Nck2 siRNA undifferentiated and differentiated 3T3-L1 cells (n = 3) (*B*). Oleate-induced lipid droplet formation in control and Nck2 siRNA 3T3-L1 preadipocytes (*C*). Confocal images were taken at magnifications ×10 and ×40 . mRNA levels of indicated lipolytic genes in $Nck2^{+/+}$ (n = 6) and $Nck2^{-/-}$ (n = 5) WAT SVF after 7 days of differentiation (*D*) and control and Nck2 siRNA undifferentiated and differentiated 3T3-L1 cells (n = 3) (*E*). Body (n = 13) and adipose tissue weights (n = 4) of $Nck2^{+/+}$ and $Nck2^{-/-}$ mice fed or fasted for 24 h (n = 5) and 48 h (n = 4) (*F*). Fed blood levels of TGs 24 weeks postweaning (*G*) and NEFAs at indicated ages (*H*) in $Nck2^{+/+}$ (n = 10–22) and $Nck2^{-/-}$ (n = 10–25) mice. Data are mean ± SEM. *P < 0.05, **P < 0.01 by unpaired Student t test. siCTL, control siRNA; siNck2, Nck2 siRNA.

Nck2 Deficiency Promotes PERK Activation and Signaling

The UPR is essential during adipogenesis (30–32). We and others previously demonstrated that Nck1, which shares a high level of identity with Nck2, regulates the IRE1α and PERK arms of the UPR (6–8). Therefore, we hypothesized that enhanced adipogenesis induced by Nck2 deficiency in adipocyte precursors is UPR dependent. Accordingly, *Atf4* and *Ddit3* (CHOP) mRNA levels were significantly further increased in Nck2-silenced 3T3-L1 cells after 4 days of differentiation, whereas *uXbp1* and *sXbp1* mRNAs remained unchanged compared with control 3T3-L1 cells (Fig. 6*A*). Higher levels of ATF4 and activated PERK (Thr^{980}) were detected in Nck2-silenced 3T3-L1 adipocytes (Fig. 6*B*). Furthermore, eIF2αSer^{51} phosphorylation, a classical marker of PERK activation associated with increased ATF4, was significantly increased in $Nck2^{-/-}$ mouse eWAT (Fig. 6*C*). Altogether, these data demonstrate that Nck2 deficiency is accompanied by increased activity of the PERK-peIF2α-ATF4 pathway, which could mediate Nck2 deficiency effect on adipocyte differentiation. Supporting this hypothesis, overexpression of PERK at low levels in 3T3-L1 preadipocytes mimicked the effects of Nck2 silencing by enhancing *Pparg* and *Fabp4* mRNA levels at day 6 of differentiation (Fig. 6*D* and *E*). To further demonstrate that Nck2 deficiency involves enhanced PERK activity and signaling in promoting adipogenesis, we followed control and Nck2 siRNA 3T3-L1 cell differentiation in the presence of a potent specific PERK inhibitor (GSK2606414) at a dose that only partially inhibits thapsigargin-induced PERK activation (10 nmol/L, data not shown). As aforementioned, silencing Nck2 in 3T3-L1 cells increased expression of *Pparg* and *Fabp4* and lipid droplet formation after 4 days of differentiation (Fig. 6*F* and *G*). However, PERK inhibitor added during differentiation of 3T3-L1 cells prevented the effects of Nck2 silencing on enhanced *Pparg* and *Fabp4* mRNA levels and lipid droplet formation, but it had no effect in control 3T3-L1 cells. *Nck2* mRNA quantitative PCR analysis established that the PERK inhibitor effects were not due to Nck2 expression recovery (Fig. 6*G*). Taken together, these results provide strong evidence that the mechanism through which Nck2 deficiency leads to enhanced adipogenesis in vitro and adiposity in vivo is likely associated with primed physiological PERK activity and signaling.

Nck2$^{-/-}$ Mice Develop Progressive Glucose Intolerance and Insulin Resistance

We investigated whether enhanced adiposity accompanied by adipocyte dysfunction affects glucose homeostasis in $Nck2^{-/-}$ mice. Glucose tolerance tests revealed that $Nck2^{-/-}$ mice displayed glucose intolerance at 16 weeks postweaning, which was exacerbated in 1-year-old mice (Fig. 7*A*). As revealed by insulin tolerance tests, insulin resistance in $Nck2^{-/-}$ mice was already apparent 16 weeks postweaning and became significantly established at 24 weeks (Fig. 7*B*). Impaired glucose disposal in $Nck2^{-/-}$ mice was not due to failure of pancreatic β-cells to provide enough insulin because in vivo glucose-stimulated insulin secretion (GSIS) in $Nck2^{-/-}$ mice (Fig. 7*C*) and insulin content in islets from *Nck2*-deficient mice ($Nck2^{+/+}$ 16.4 ± 2.1 vs. $Nck2^{-/-}$ 21.3 ± 1.1 ng insulin/ng DNA, $P < 0.05$) were increased compared with respective controls. In addition, $Nck2^{-/-}$ mice displayed hyperinsulinemia from 24 weeks (Fig. 7*D*), which probably contributed to maintaining normal glycemia in $Nck2^{-/-}$ mice (Fig. 7*E*).

Finally, we compared energy metabolism and physical activity in both mouse genotypes. Clearly, no difference was observed in daily food intake, energy expenditure, and locomotor activity between genotypes (Fig. 7*F*, *G*, and *I*). However, the respiratory exchange ratio (RER) showed that $Nck2^{-/-}$ mice were significantly less effective at shifting from dark-cycle carbohydrate breakdown to lipid β-oxidation during daylight (Fig. 7*H*), making them metabolically less flexible.

Nck2$^{-/-}$ Mice Display Secondary Hepatic Steatosis

Correlating with $Nck2^{-/-}$ mice spontaneously developing whole-body insulin resistance and hyperinsulinemia, we discovered that although this was not observed at a younger age (10 weeks), $Nck2^{-/-}$ mice at 32 weeks postweaning display hepatic steatosis (Fig. 8*A*). Hepatic steatosis in $Nck2^{-/-}$ mice was not supported by changes in expression of genes regulating hepatic lipid metabolism (Fig. 8*B*). Furthermore, in vivo insulin-induced Akt phosphorylation was significantly reduced in the liver of $Nck2^{-/-}$ mice (Fig. 8*C*), whereas no change in insulin-induced Akt phosphorylation was detected in muscle and eWAT (data not shown). In agreement with hepatic insulin resistance, $Nck2^{-/-}$ mice also displayed increased hepatic gluconeogenesis in the pyruvate tolerance test (Fig. 8*D*), higher expression of the PEPCK implicated in gluconeogenesis (Fig. 8*E*), and lower glycogen content (Fig. 8*F*). Lipid accumulation in skeletal muscle was not apparent (data not shown), and glycogen content was unchanged (Fig. 8*F*), further supporting unaltered insulin sensitivity in this tissue.

To determine whether hepatic insulin resistance in $Nck2^{-/-}$ mice is due to impaired autonomous hepatocyte function, we assessed insulin-induced phosphorylation of Akt in primary hepatocytes in culture. Of note, insulin response in $Nck2^{-/-}$ primary hepatocytes appeared to be increased compared with control hepatocytes (Fig. 8*G*), indicating that hepatic insulin resistance in $Nck2^{-/-}$ mice results from a systemic effect instead of being hepatocyte autonomous. Globally, *Nck2* deficiency in mice induces progressive metabolic disorders that are consistent with enhanced adiposity and circulating lipids associated with dysregulated adipogenesis and adipocyte function.

DISCUSSION

In this study, we uncovered an unexpected role for the SH domains containing adaptor Nck2 in regulating adipogenesis and adipocyte function associated with the control of glucose homeostasis. We identified *Nck2*-deficient mice

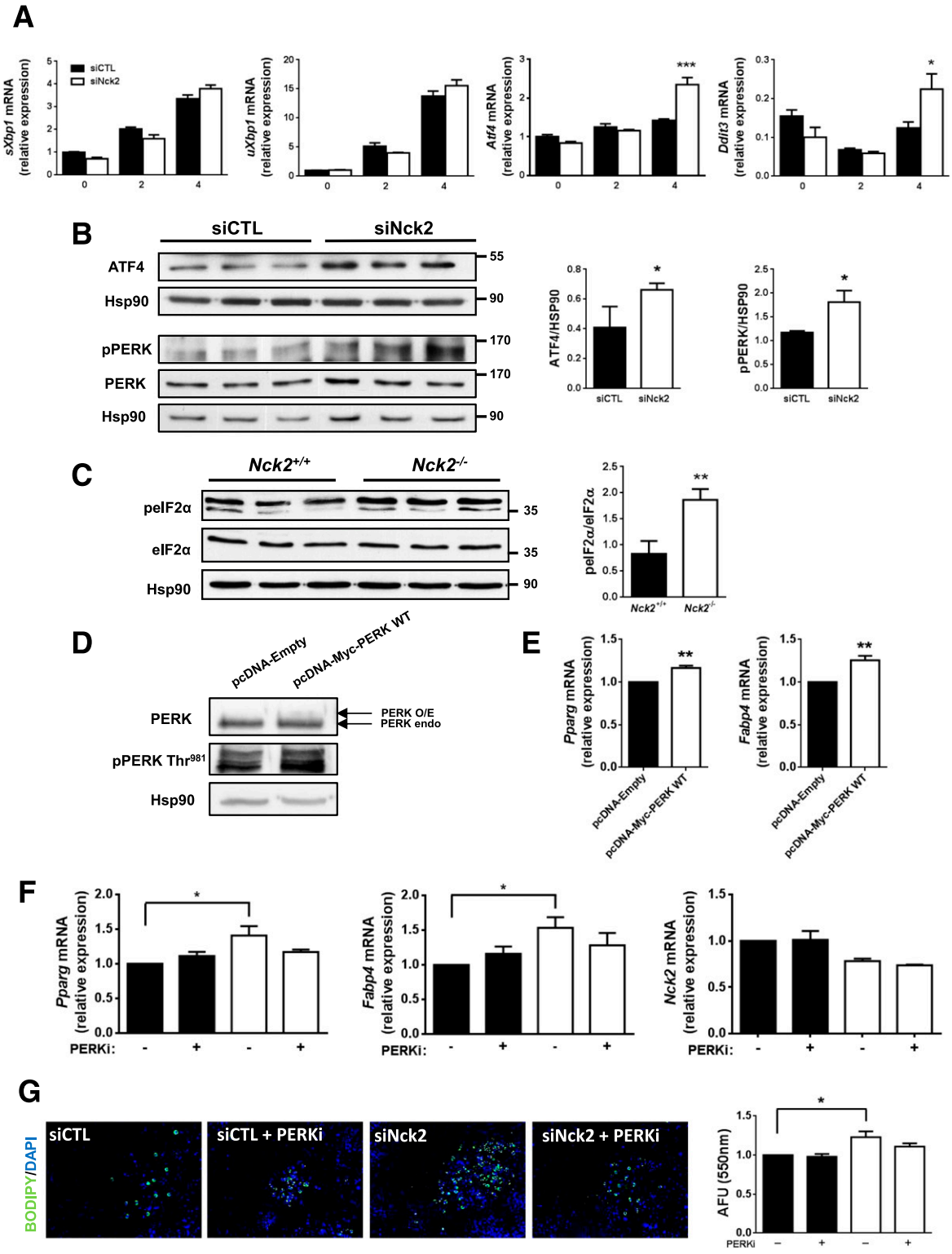

Figure 6—Nck2 deficiency promotes PERK activation and signaling during adipocyte differentiation. mRNA levels of indicated UPR markers in control and Nck2 siRNA-treated 3T3-L1 cells during differentiation (n = 3) (*A*). ATF4 and PERK Thr^{980} phosphorylation levels in control and Nck2 siRNA 3T3-L1 cells after 4 days of differentiation (n = 3) (*B*). eIF2αSer^{51} phosphorylation in indicated eWAT from 8-week-old mice (*C*). Western blots showing PERK overexpression and activation and Hsp90 as loading control in 3T3-L1 cells (*D*). Expression of *Pparg* and *Fabp4* mRNA levels after 6 days of differentiation in 3T3-L1 cells overexpressing PERK (*E*). Effect of PERK inhibitor on *Pparg*, *Fabp4*, and *Nck2* mRNA levels (n = 3) and lipid droplet formation (confocal images magnification ×10) in differentiated control and Nck2 siRNA-treated 3T3-L1 cells (n = 4) (*F* and *G*). Data are mean ± SEM. *P < 0.05, **P < 0.01, ***P < 0.001 by unpaired Student t test. AFU, arbitrary fluorescent unit; O/E, overexpression; PERK endo, endogenous PERK; PERKi, PERK inhibitor; siCTL, control siRNA; siNck2, Nck2 siRNA.

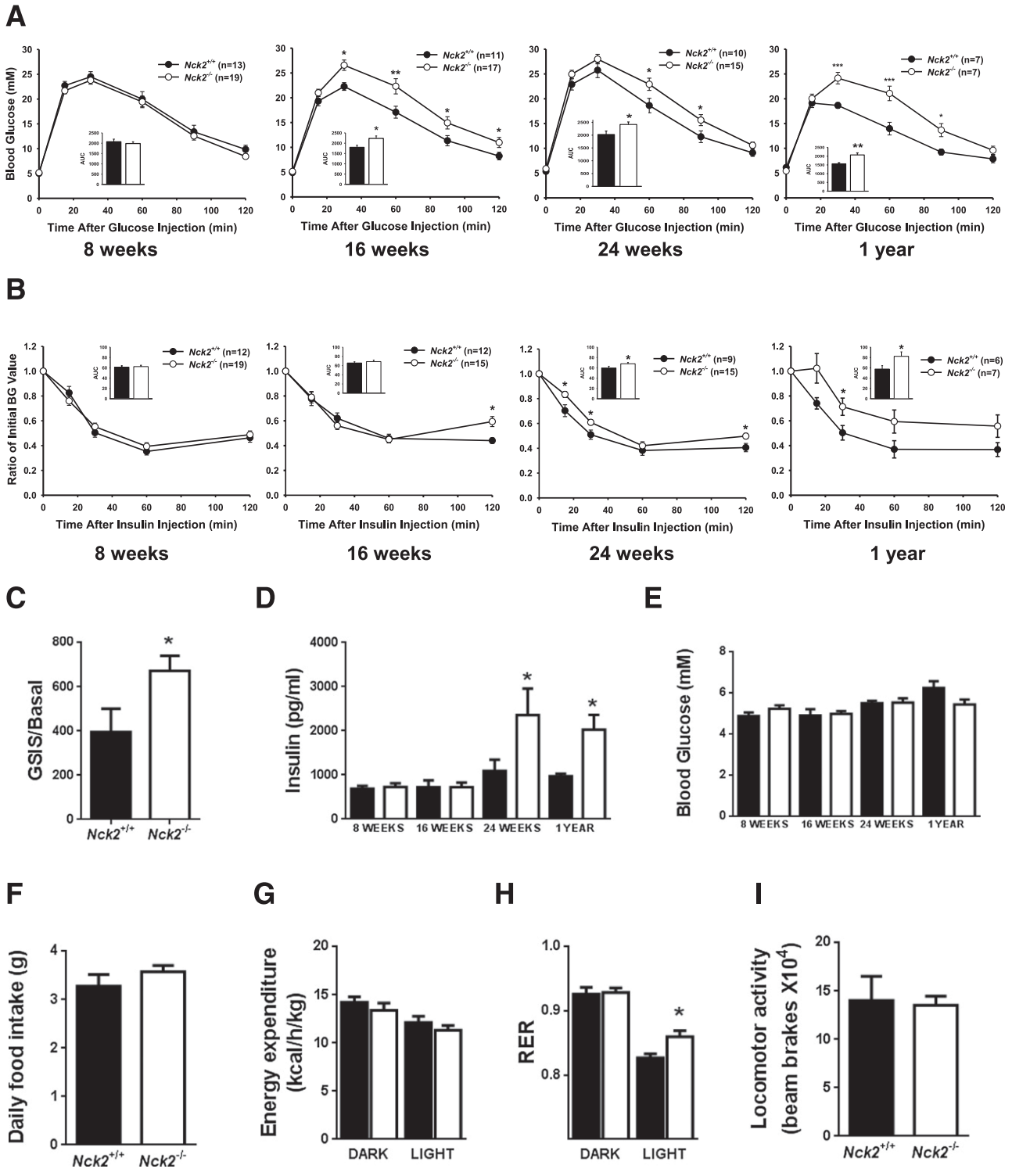

Figure 7—*Nck2*$^{-/-}$ mice developed progressive glucose intolerance and insulin resistance. Glucose (*A*) and insulin (*B*) tolerance tests in mice. Insets show AUC. In vivo GSIS (n = 6) (*C*), fed insulin (*D*), and fasted glucose (*E*) levels in *Nck2*$^{+/+}$ (n = 4–11) and *Nck2*$^{-/-}$ (n = 7–17) mice. Metabolic parameters were daily food intake (*F*), energy expenditure (*G*), RER (*H*), and locomotor activity (*I*) in *Nck2*$^{+/+}$ (n = 4) and *Nck2*$^{-/-}$ mice (n = 7). Solid bars, *Nck2*$^{+/+}$ mice; open bars, *Nck2*$^{-/-}$ mice. Data are mean ± SEM. *P < 0.05, **P < 0.01, ***P < 0.001 by two-way ANOVA (*A* and *B*) and unpaired Student t test (*C*–*I*). AUC, area under the curve; BG, blood glucose.

as a model displaying spontaneous increased adiposity and dysfunctional adipocytes concomitant with progressive glucose intolerance, insulin resistance, and hepatic steatosis. Correlating with high Nck2 expression in WAT, *Nck2*-deficient mice were found to be more susceptible to expanded WAT. Consistently, we demonstrate reduced Nck2 expression in oWAT of severely obese human subjects, supporting the existence of a negative relationship between WAT

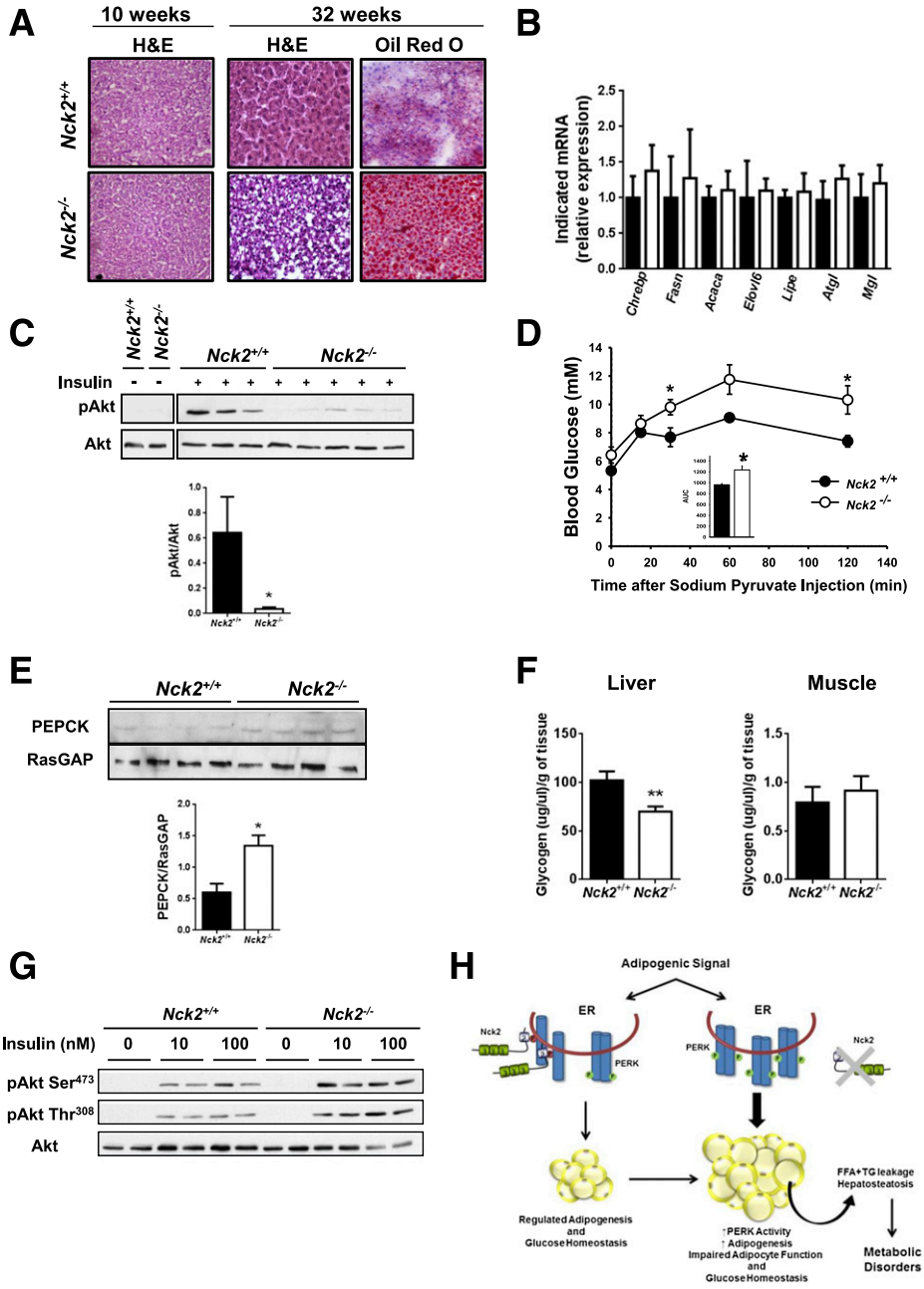

Figure 8—*Nck2*$^{-/-}$ mice display hepatic steatosis. Liver H&E and ORO staining at indicated ages (original magnification ×20) (n = 3) (*A*). Hepatic lipogenic and lipolytic gene expression in indicated mice at 24 weeks postweaning. Solid bars, *Nck2*$^{+/+}$ mice; open bars, *Nck2*$^{-/-}$ mice (*B*). In vivo insulin-induced pAkt in liver (*C*). Pyruvate challenge test in indicated mice (1 year). Inset shows AUC (n = 6) (*D*). Hepatic PEPCK protein levels (*E*). Hepatic and skeletal muscle glycogen content at 24 weeks postweaning (*Nck2*$^{+/+}$ n = 6, *Nck2*$^{-/-}$ n = 7) (*F*). Insulin-induced pAkt in primary hepatocytes (*G*). Model illustrating how Nck2 deficiency leads to altered WAT homeostasis by priming physiological PERK activity and signaling (*H*). Data are mean ± SEM. *P < 0.05, **P < 0.01 by unpaired Student t test (*E* and *F*) or two-way ANOVA (*D*). AUC, area under the curve; FFA, free fatty acid.

Nck2 expression and BMI in humans. The success of existing pharmacological approaches combined with caloric restriction and increased physical activity to facilitate weight loss in humans is still limited and accompanied by major secondary effects that dampen their clinical potential in treating obesity. The current study in mice and humans suggests that moving forward in developing strategies to modulate Nck2 expression could be a valuable alternative to specifically control the pathological visceral WAT expansion that leads to obesity.

In *Nck2*-deficient mice, increased adiposity is characterized by adipocyte hypertrophy, but increased levels of circulating lipids indicate dysfunctional adipocytes. Upregulated expression of lipogenic enzymes in *Nck2*-deficient adipocytes suggest that an increased rate of lipogenesis could contribute to adipocyte hypertrophy

and exceed the maximum adipocyte lipid storage capacity. Moreover, enhanced lipolysis in *Nck2*-deficient mice could significantly contribute to increased levels of circulating lipids, explaining why *Nck2*-deficient mice develop hepatic steatosis. In parallel, RNASeq of differentially expressed genes in $Nck2^{-/-}$ eWAT mice suggests that upregulated expression of ECM genes, promoting WAT ECM stiffness and fibrosis (33), could contribute to mature adipocyte dysfunction. Although ECM gene regulation is interesting, fold induction of ECM genes appears less pronounced than other genes reported. Therefore, further investigation is required to assess whether Nck2 deficiency affects mature adipocyte function through ECM-related fibrosis.

The current study provides strong evidence that increased fat mass in *Nck2*-deficient mice is associated with not only adipocyte hypertrophy resulting from impaired lipid metabolism in adipocytes, but also enhanced adipogenesis. Genes encoding players of the Wnt signaling reported to inhibit adipocyte differentiation (34) were strongly downregulated in *Nck2*-deficient eWAT, which thereby could significantly contribute to enhanced adipogenesis. Consistent with a role for Nck2 in limiting adipogenesis, Nck2 deficiency promotes differentiation of preadipocytes into adipocytes in vitro.

We previously reported that the PERK-peIF2α-ATF4 pathway is damped following overexpression of either Nck1 or Nck2 in various mammalian cells (12,13), revealing that both Nck1 and Nck2 are negative regulators of PERK signaling in multiple models. Accordingly, Nck2 deficiency enhances physiological PERK activation and signaling during adipocyte differentiation and in mature adipocytes. Consistent with PPARγ being a direct target of ATF4 and ATF4 overexpression in 3T3-L1 preadipocytes enhancing differentiation (35), the current findings that PPARγ and phosphorylation of $eIF2\alpha Ser^{51}$ are significantly increased in *Nck2*-deficient eWAT further support enhanced PERK activation and signaling. We provided strong mechanistic evidence that physiological PERK activity and signaling regulate adipocyte differentiation and mediate Nck2 deficiency effect on adipogenesis in vitro and adipogenesis leading to increased adiposity in vivo (Fig. 8*H*). Previous studies reported that the UPR is activated in adipose tissue of obese patients without diabetes in relation with BMI (36) and in obese subjects with insulin resistance (37), suggesting a link between activated UPR and WAT mass expansion. We confirmed activation of PERK and IRE1α signaling during adipocyte differentiation. However, silencing Nck2 in preadipocytes has no further effect on the IRE1α-XBP1 pathway, suggesting that although Nck2 specifically modulates the PERK-peIF2α-ATF4 pathway during adipocyte differentiation, it has no control over IRE1α signaling in this context.

The exact mechanism by which silencing Nck2 promotes PERK activation and signaling during adipocyte differentiation still remains to be determined. We have identified Nck1 as a negative regulator of PERK activation through its direct interaction with PERK (13). In agreement with Nck2 also directly interacting with PERK (13), we provided strong evidence that silencing Nck2 in preadipocytes promotes adipogenesis by further enhancing PERK activation and signaling during this process (30).

Earlier studies proposed that Nck1 and Nck2 are functionally redundant because double knockout of *Nck1* and *Nck2* in mice is embryonically lethal, whereas individual *Nck* knockout shows no apparent phenotype (16). Although Nck1 and Nck2 share common functions and interacting proteins (38), studies have reported specific functions and exclusive binding partners for Nck proteins (39–41). In agreement, we showed that *Nck1*-deficient mice display normal glucose homeostasis (15), and in the current study, we report that *Nck2*-deficient mice spontaneously develop progressive increased adiposity concomitant with impaired glucose homeostasis, insulin resistance, and hepatic steatosis. Although $Nck2^{-/-}$ mice were generated a while ago and have been reported with no obvious phenotype (16), progressive adiposity was probably missed because it requires careful WAT investigation given that mouse body weight was not affected.

In summary, this study using in vivo *Nck2* deficiency and in vitro Nck2 silencing in preadipocytes argues for an unanticipated role of Nck2 in controlling the susceptibility of developing adiposity. Furthermore, the study unveils the importance of Nck2 and the regulation of PERK as potential new avenues for managing obesity in humans.

Acknowledgments. The authors thank T. Pawson (Mount Sinai Hospital, Toronto, Ontario, Canada) for providing $Nck2^{+/-}$ mice several years ago. From McGill University and the McGill University Health Centre Research Institute, the authors also thank Victor Dumas for technical assistance, E.C. Davis for histological analysis, M. Kokoeva for metabolic studies, S. Chevalier for expertise in NEFA determination, the immunophenotyping platform for flow cytometry expertise, and S.A. Laporte and J.J. Bergeron for critical reading of the manuscript. Finally, the authors acknowledge the surgery team, bariatric surgeons, and Biobank staff of the IUCPQ.

Funding. J.D. was supported by postdoctoral fellowships from the Fonds de la Recherche du Québec en Santé and the Canadian Diabetes Association. J.-F.C. is a recipient of a senior career award from the Fonds de la Recherche du Québec en Santé. J.-F.C. and L.L. have received funds from the Canadian Institutes of Health Research (MOP-144425 and MOP-115045, respectively).

Duality of Interest. No potential conflicts of interest relevant to this article were reported.

Author Contributions. J.D. contributed to the experimental design, data collection, data interpretation and analysis, preparation of figures, and writing of the manuscript. B.L. contributed to the experiments and critical reading of the manuscript. N.H. contributed to the experiments. M.-A.G. contributed to the RNASeq analysis. J.-F.C. contributed to the RNASeq analysis and critical reading of the manuscript. L.L. contributed to study design and final editing of the manuscript. L.L. is the guarantor of this work and, as such, had full access to all the data in the study and takes responsibility for the integrity of the data and the accuracy of the data analysis.

References

1. Sun K, Kusminski CM, Scherer PE. Adipose tissue remodeling and obesity. J Clin Invest 2011;121:2094–2101

2. Fox CS, Heard-Costa N, Cupples LA, Dupuis J, Vasan RS, Atwood LD. Genome-wide association to body mass index and waist circumference: the Framingham Heart Study 100K project. BMC Med Genet 2007;8(Suppl. 1):S18
3. Chen M, She H, Davis EM, et al. Identification of Nck family genes, chromosomal localization, expression, and signaling specificity. J Biol Chem 1998; 273:25171–25178
4. Coppolino MG, Krause M, Hagendorff P, et al. Evidence for a molecular complex consisting of Fyb/SLAP, SLP-76, Nck, VASP and WASP that links the actin cytoskeleton to Fcgamma receptor signalling during phagocytosis. J Cell Sci 2001;114:4307–4318
5. Jones N, Blasutig IM, Eremina V, et al. Nck adaptor proteins link nephrin to the actin cytoskeleton of kidney podocytes. Nature 2006;440:818–823
6. Kebache S, Cardin E, Nguyên DT, Chevet E, Larose L. Nck-1 antagonizes the endoplasmic reticulum stress-induced inhibition of translation. J Biol Chem 2004;279:9662–9671
7. Nguyên DT, Kebache S, Fazel A, et al. Nck-dependent activation of extracellular signal-regulated kinase-1 and regulation of cell survival during endoplasmic reticulum stress. Mol Biol Cell 2004;15:4248–4260
8. Rajesh K, Iyer A, Suragani RN, Ramaiah KV. Intersubunit and interprotein interactions of alpha- and beta-subunits of human eIF2: effect of phosphorylation. Biochem Biophys Res Commun 2008;374:336–340
9. Walter P, Ron D. The unfolded protein response: from stress pathway to homeostatic regulation. Science 2011;334:1081–1086
10. Kebache S, Zuo D, Chevet E, Larose L. Modulation of protein translation by Nck-1. Proc Natl Acad Sci U S A 2002;99:5406–5411
11. Gandin V, Masvidal L, Cargnello M, et al. mTORC1 and CK2 coordinate ternary and eIF4F complex assembly. Nat Commun 2016;7:11127
12. Latreille M, Larose L. Nck in a complex containing the catalytic subunit of protein phosphatase 1 regulates eukaryotic initiation factor 2alpha signaling and cell survival to endoplasmic reticulum stress. J Biol Chem 2006;281:26633–26644
13. Yamani L, Latreille M, Larose L. Interaction of Nck1 and PERK phosphorylated at Y^{561} negatively modulates PERK activity and PERK regulation of pancreatic β-cell proinsulin content. Mol Biol Cell 2014;25:702–711
14. Yamani L, Li B, Larose L. Nck1 deficiency improves pancreatic β cell survival to diabetes-relevant stresses by modulating PERK activation and signaling. Cell Signal 2015;27:2555–2567
15. Latreille M, Laberge MK, Bourret G, Yamani L, Larose L. Deletion of Nck1 attenuates hepatic ER stress signaling and improves glucose tolerance and insulin signaling in liver of obese mice. Am J Physiol Endocrinol Metab 2011;300: E423–E434
16. Bladt F, Aippersbach E, Gelkop S, et al. The murine Nck SH2/SH3 adaptors are important for the development of mesoderm-derived embryonic structures and for regulating the cellular actin network. Mol Cell Biol 2003;23:4586–4597
17. Li H, Dusseault J, Larose L. Nck1 depletion induces activation of the PI3K/Akt pathway by attenuating PTP1B protein expression. Cell Commun Signal 2014; 12:71
18. Mounier C, Dumas V, Posner BI. Regulation of hepatic insulin-like growth factor-binding protein-1 gene expression by insulin: central role for mammalian target of rapamycin independent of forkhead box O proteins. Endocrinology 2006; 147:2383–2391
19. Yang W, Thein S, Wang X, et al. BSCL2/seipin regulates adipogenesis through actin cytoskeleton remodelling. Hum Mol Genet 2014;23:502–513
20. Huang W, Sherman BT, Lempicki RA. Systematic and integrative analysis of large gene lists using DAVID bioinformatics resources. Nat Protoc 2009;4:44–57
21. Huang W, Sherman BT, Lempicki RA. Bioinformatics enrichment tools: paths toward the comprehensive functional analysis of large gene lists. Nucleic Acids Res 2009;37:1–13
22. Subramanian A, Tamayo P, Mootha VK, et al. Gene set enrichment analysis: a knowledge-based approach for interpreting genome-wide expression profiles. Proc Natl Acad Sci U S A 2005;102:15545–15550
23. Peyot ML, Nolan CJ, Soni K, et al. Hormone-sensitive lipase has a role in lipid signaling for insulin secretion but is nonessential for the incretin action of glucagon-like peptide 1. Diabetes 2004;53:1733–1742
24. Takahashi M, Kamei Y, Ezaki O. Mest/Peg1 imprinted gene enlarges adipocytes and is a marker of adipocyte size. Am J Physiol Endocrinol Metab 2005; 288:E117–E124
25. Laplante M, Horvat S, Festuccia WT, et al. DEPTOR cell-autonomously promotes adipogenesis, and its expression is associated with obesity. Cell Metab 2012;16:202–212
26. Morton NM, Nelson YB, Michailidou Z, et al. A stratified transcriptomics analysis of polygenic fat and lean mouse adipose tissues identifies novel candidate obesity genes. PLoS One 2011;6:e23944
27. Bennett CN, Ross SE, Longo KA, et al. Regulation of Wnt signaling during adipogenesis. J Biol Chem 2002;277:30998–31004
28. Ross SE, Hemati N, Longo KA, et al. Inhibition of adipogenesis by Wnt signaling. Science 2000;289:950–953
29. Mori H, Prestwich TC, Reid MA, et al. Secreted frizzled-related protein 5 suppresses adipocyte mitochondrial metabolism through WNT inhibition. J Clin Invest 2012;122:2405–2416
30. Han J, Murthy R, Wood B, et al. ER stress signalling through eIF2α and CHOP, but not IRE1α, attenuates adipogenesis in mice. Diabetologia 2013;56: 911–924
31. Lowe CE, Dennis RJ, Obi U, O'Rahilly S, Rochford JJ. Investigating the involvement of the ATF6α pathway of the unfolded protein response in adipogenesis. Int J Obes 2012;36:1248–1251
32. Sha H, He Y, Chen H, et al. The IRE1alpha-XBP1 pathway of the unfolded protein response is required for adipogenesis. Cell Metab 2009;9:556–564
33. Reggio S, Rouault C, Poitou C, et al. Increased basement membrane components in adipose tissue during obesity: links with TGFβ and metabolic phenotypes. J Clin Endocrinol Metab 2016;101:2578–2587
34. Laudes M. Role of WNT signalling in the determination of human mesenchymal stem cells into preadipocytes. J Mol Endocrinol 2011;46:R65–R72
35. Yu K, Mo D, Wu M, et al. Activating transcription factor 4 regulates adipocyte differentiation via altering the coordinate expression of CCATT/enhancer binding protein β and peroxisome proliferator-activated receptor γ. FEBS J 2014;281:2399–2409
36. Sharma NK, Das SK, Mondal AK, et al. Endoplasmic reticulum stress markers are associated with obesity in nondiabetic subjects. J Clin Endocrinol Metab 2008;93:4532–4541
37. Boden G, Duan X, Homko C, et al. Increase in endoplasmic reticulum stress-related proteins and genes in adipose tissue of obese, insulin-resistant individuals. Diabetes 2008;57:2438–2444
38. Labelle-Cote M, Dusseault J, Ismail S, Picard-Cloutier A, Siegel PM, Larose L. Nck2 promotes human melanoma cell proliferation, migration and invasion in vitro and primary melanoma-derived tumor growth in vivo. BMC Cancer 2011; 11:443
39. Guan S, Fan J, Han A, Chen M, Woodley DT, Li W. Non-compensating roles between Nckalpha and Nckbeta in PDGF-BB signaling to promote human dermal fibroblast migration. J Invest Dermatol 2009;129:1909–1920
40. Mukherjee C, Bakthavachalu B, Schoenberg DR. The cytoplasmic capping complex assembles on adapter protein nck1 bound to the proline-rich C-terminus of Mammalian capping enzyme. PLoS Biol 2014;12:e1001933
41. Ngoenkam J, Paensuwan P, Preechanukul K, et al. Non-overlapping functions of Nck1 and Nck2 adaptor proteins in T cell activation. Cell Commun Signal 2014;12:21